PILE RESPONSE DURING EARTHQUAKE AND PERFORMANCE EVALUATION OF PILE FOUNDATION

Yuji MIYAMOTO

Kobori Research Complex, Kajima Corporation, Tokyo, Japan
E-mail: miyamoto@krc.kajima.co.jp

ABSTRACT

Pile foundation response during earthquakes is strongly affected by nonlinear soil-pile foundation interaction. The damages to pile foundations during the Hyogo-ken Nanbu earthquake of 1995 were obviously attributed to nonlinear interaction of soil-pile foundation-superstructure. Dynamic centrifuge tests are performed on a four-pile group foundation model embedded in saturated fine sand layers. The pile foundation model is excited by a shaking table at the pile tip and by lateral loading at the pile head to investigate the effect of inertia force and soil displacement, respectively, on pile bending moments. The inertial and kinematic pile bending moments are compared with analytical results. Next, earthquake response analyses are conducted to clarify the effect of the nonlinear soil-pile foundation-superstructure system on performance of pile foundation. Pile bending moments are calculated using the nonlinear relationship between bending moment and curvature dependent on axial force. Performance evaluation of the pile foundation is discussed on the basis of pile curvature and pile foundation deformation.

KEYWORDS

pile foundation; nonlinear interaction; centrifuge test; liquefaction; pile bending moment
pile group effect; axial force in pile; performance design; performance evaluation

1. INTRODUCTION

For implementation of performance-based design, it is necessary to precisely predict a structure response during an earthquake. Pile foundation response, however, is very complicated because of pile group effects and nonlinear interactions of soil and superstructure [1], [2], [3]. In this paper, pile foundation responses are clarified by dynamic centrifuge tests and nonlinear analyses of the soil-pile foundation-superstructure system. The dynamic centrifuge tests are performed on the pile foundation model in liquefiable soil to study the pile bending moment induced by the inertial and kinematic interactions. The pile foundation model is excited by a shaking table and by lateral loading at the pile head. Correlation analyses are conducted to verify the numerical model with beam-nonlinear interaction springs. Further, nonlinear analyses are conducted to study the performance of the pile foundation on the basis of pile curvature and pile foundation deformation.

2. CENTRIFUGE MODEL TEST

2.1 Centrifuge test equipment and conditions

The shaking table test and the lateral loading test were performed under a centrifugal acceleration of 45g [4]. A geotechnical centrifuge with a maximum radius of 3.0m was employed. The lateral loading system is consisted of a hydraulic piston and could be controlled in terms of both displacement and load.

Figure 1 shows the centrifuge test model with the positions of measuring instruments within a laminar container. The dimensions in Figure 1 are given in prototype scale, which is 45 times the model scale. The laminar box had inside dimensions of length L=50cm, width W=20cm and height H=48cm. The pile foundation model was set up in saturated Toyoura sand deposits. The sand deposits were prepared by dry pluviation in the laminar box, and then saturated by introducing pore fluid from the bottom. Silicon oil, which has a viscosity 50 times that of water, was used as the pore fluid. The pile foundation model consisted of a four-pile group and a rigid pile cap that represented the inertial mass of the superstructure. The model piles represented prototype tubular-steel piles

0.7m in diameter and 20.7m long, with a wall thickness of 14mm. The flexural rigidity of the pile was 1.21×10^5t m^2. Pile spacing was 5.3 times pile diameter. The piles were rigidly connected to the pile cap.
The test cases are summarized in Figure 2. The NS component of El Centro 1940 with 173.5Gal maximum acceleration was used as the input wave for Test-A. The displacement time history of the pile cap obtained for Test-A was used as the input wave for Test-B.

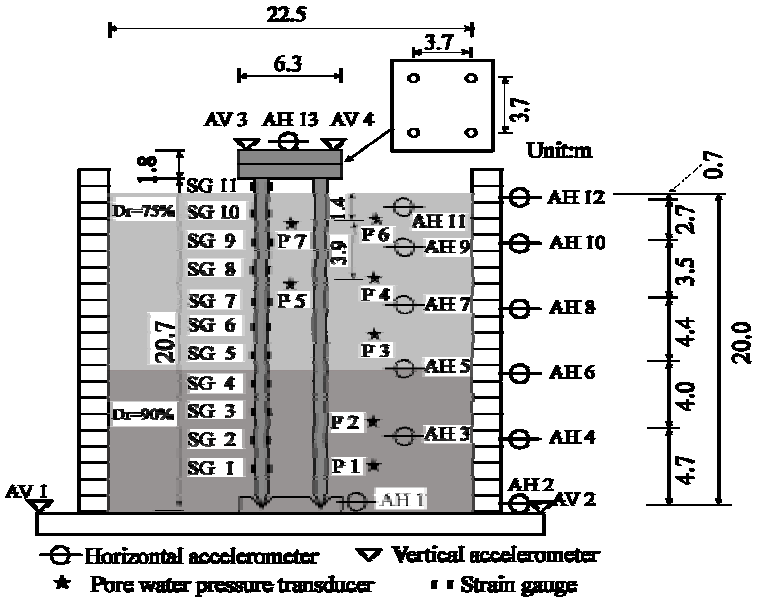

Figure 1: Centrifuge test model and measuring instruments (indicated in prototype scale)

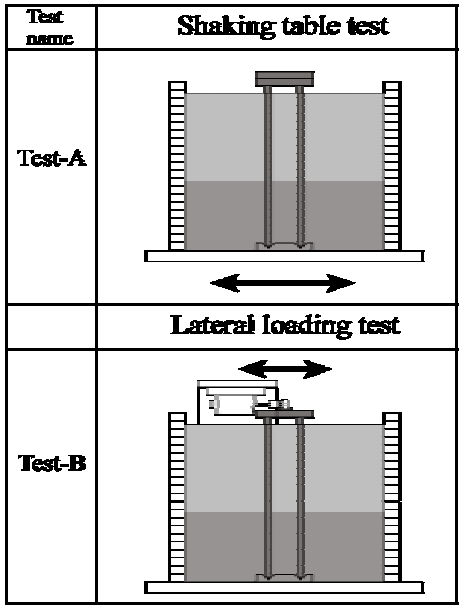

Figure 2: Test cases

2.2 Numerical model

Correlation analyses were carried out using a beam-interaction spring model, as shown in Figure 3. The interaction springs employed in this analytical model were not Winkler type spring, but consisted of lateral and shear soil springs. The pile foundation was idealized by a one-stick model with lumped masses and beam elements. The lumped masses were connected to the free field soil through nonlinear lateral interaction springs modified at each step in accordance with the generation and dissipation of excess pore water pressures. For simplicity, this analytical model did not adopt additive masses of the soil. Analyses of the seismic response of the soil-pile foundation system were conducted in the following two stages. Firstly, the free-field soil responses were calculated by nonlinear effective stress analysis, using the computer code YUSAYUSA [5]. Then, the obtained displacement and excess pore water pressure time histories at each depth were applied through the corresponding nonlinear lateral interaction soil springs. A linear rotational spring related to the axial stiffness of the piles was also incorporated at the pile head.
The initial values of interaction soil springs should be evaluated in the linear range of soil considering pile group effects [2], [3]. Thus, the lateral load-displacement relationship of n- piles was strictly obtained using Green's functions by ring loads in three-dimensional layered stratum [6].

$$\{P\} = [K_{pp}]\ \{u\} \qquad (1)$$

where $\{P\}$ and $\{u\}$ are the vectors of loads and lateral displacements at m-nodes of each pile. A complete spring $[K_{pp}]$ is an m.n$\times$m.n interaction soil stiffness matrix of a pile group. For simplicity, $[K_{pp}]$ can be reduced to the m$\times$m matrix $[K_p]$ assuming that the displacement of each pile is identical at the same depth. Considering the displacement modes shown in Figure 4, $[K_p]$ is separated into lateral soil springs $[K_{a0}]$ and the shear soil springs $[K_{b0}]$ [2], [3].

$$\{F\} = [K_p]\ \{U\} = \{\ [K_{a0}] + [K_{b0}]\ \}\{U\} \qquad (2)$$

where

$$[K_{a0}] = \begin{bmatrix} K_{a0}^1 & & & & \\ & K_{a0}^2 & & & \\ & & \cdot & & \\ & & & K_{a0}^i & \\ & & & & \cdot \\ & & & & K_{a0}^m \end{bmatrix}, \quad [K_{b0}] = \begin{bmatrix} \square & & & \\ & \cdot & & \\ & & \cdot & \\ & & & \square \end{bmatrix}, \quad \square = K_{b0}^i \begin{bmatrix} 1 & - \\ -1 & \end{bmatrix}$$

and {F} and {U} are the vectors of lateral loads and displacements at the nodes corresponding to the depths of the lumped masses. The initial lateral and shear soil springs were calculated at low frequency (f=0.1Hz). The nonlinearity of the soil springs was assumed as shown in Figure 5. The load-displacement relationship was idealized by applying the Hardin-Drnevich model with the Masing rule. The ultimate soil resistance P_{amax0} of the lateral soil spring at each depth was evaluated after Broms [7] as shown in equation (3). The ultimate soil resistance P_{bmax0} of the shear soil spring at each depth was evaluated from equation (4).

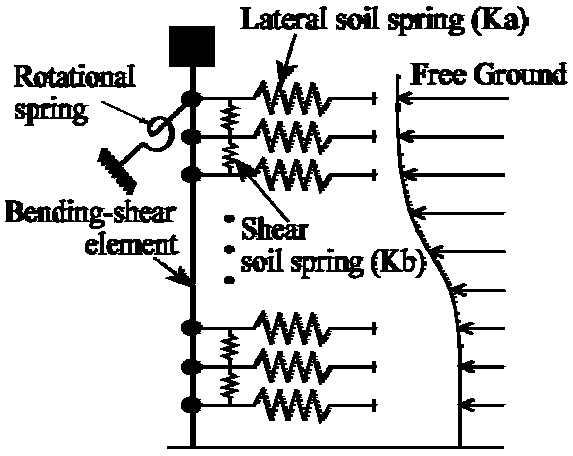

Figure 3: Numerical model of soil-pile foundation-superstructure system

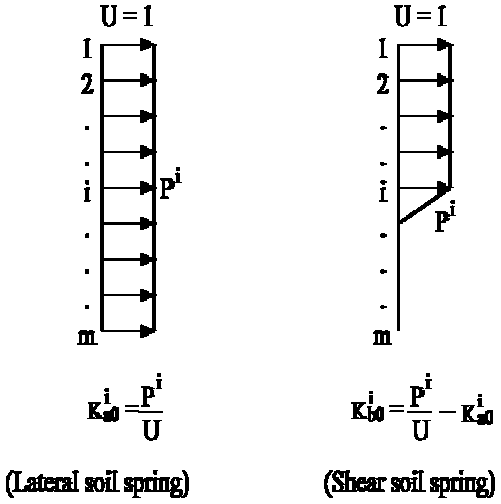

Figure 4: Reduction of the interaction spring [Kp] to the lateral [Ka] and shear [Kb] soil springs

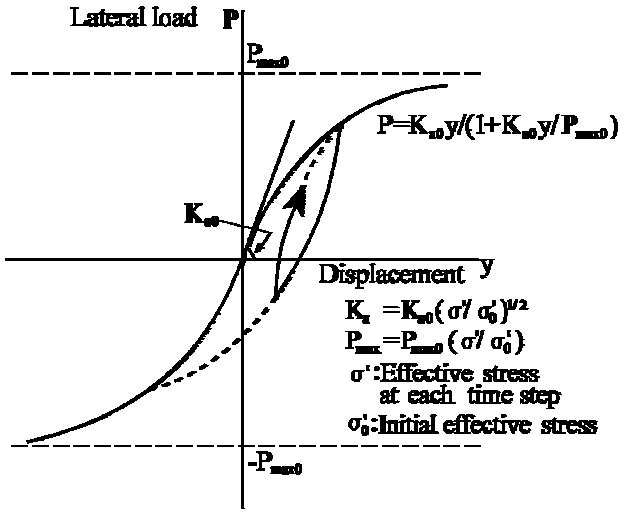

Figure 5: Nonlinear lateral load-displacement relationship of soil spring

$$P_{amax0} = 3\sigma_0 K_p dln \quad \text{(Sand)}, \qquad P_{amax0} = 9Cudln \quad \text{(Clay)} \tag{3}$$

$$P_{bmax0} = \tau_{max}.S, \qquad S = K_{b0} l/G \tag{4}$$

where $K_p=(1+\sin\phi)/(1-\sin\phi)$, ϕ is internal friction angle of the sand, Cu is undrained shear strength, $\tau_{max}=\sigma_0 \tan\phi+Cu$, S is effective area of pile foundation, G is shear modulus of soil, d is pile diameter, l is pile length equivalent to the i-th node and n is the number of piles. The soil springs and the ultimate lateral soil resistances were also modified in accordance with the generation and dissipation of excess pore water pressures at each depth. The physical properties of Toyoura sand are summarized in Table 1.

Table 1: Physical constants of Toyoura sand

Specific Gravity	Gs :	2.64	
Maximum Void Ratio	e_{max} :	0.977	
Minimum Void Ratio	e_{min} :	0.605	
Relative Density	Dr :	75%	90%
Permeability (m/sec)	kv :	1.57×10^{-4}	1.53×10^{-4}
Internal Friction Angle	ϕ :	38.2°	40.2°
Coeff. of Earth Pressure at Rest K_0	:	0.38	0.36
Initial Shear Modulus (tf/m^2)	G_0 :	965~4950	5630~7440
Parameters of YUSA YUSA			
Bp=2.00 Bu=0.90 θ s=22.0 κ=0.06			

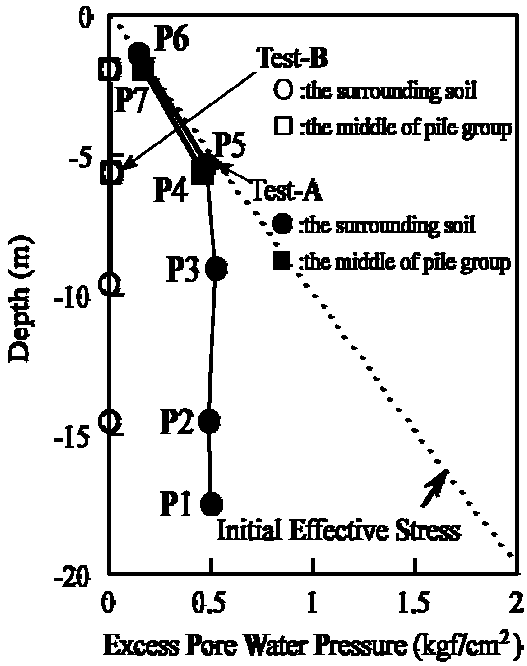

Figure 6: Comparisons of the excess pore water pressures in Test-A and Test-B

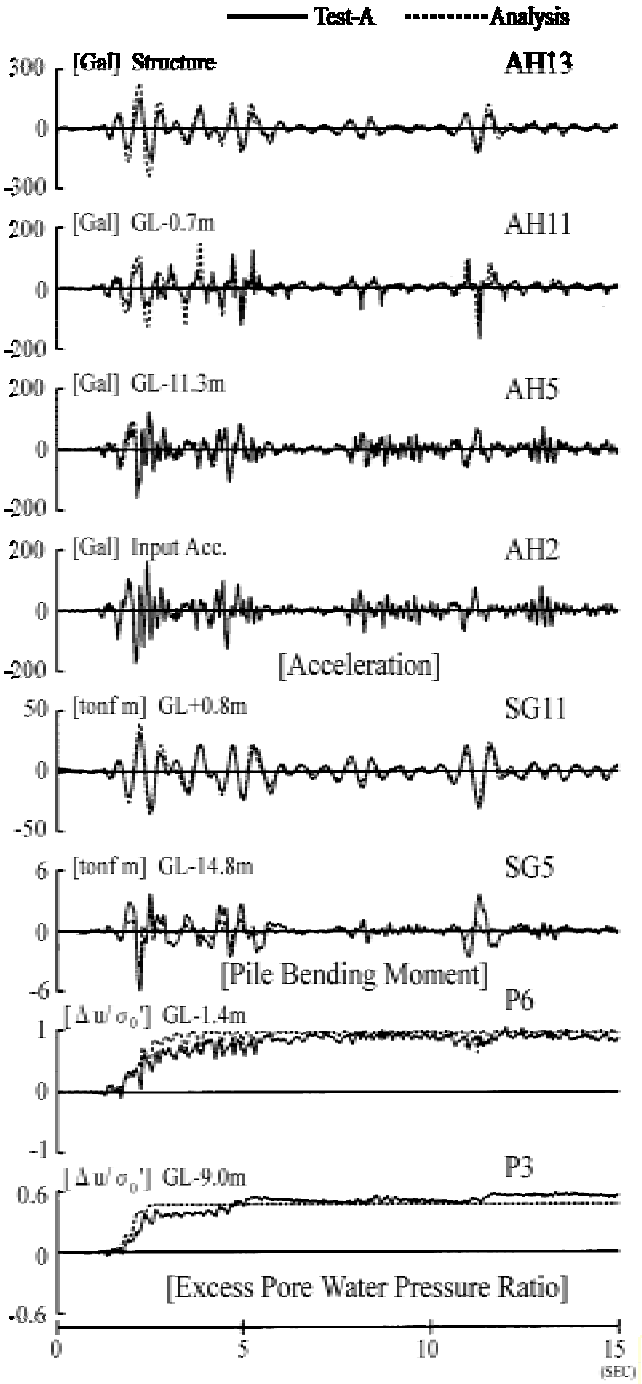

Figure 7: Comparisons of the time histories of the analyses and Test-A

2.3 Test and correlation analyses

The results described below are given in prototype scale. Figure 6 compares maximum excess pore water pressures in the surrounding soil (P1, P2, P3, P4, P6) and in the middle of the pile group (P5, P7) with the initial effective stresses for Test-A and Test-B. In Test-A, the upper 6m of the soil was completely liquefied. In Test-B, pore water pressure did not increase at each depth because the nonlinearity of the soil can

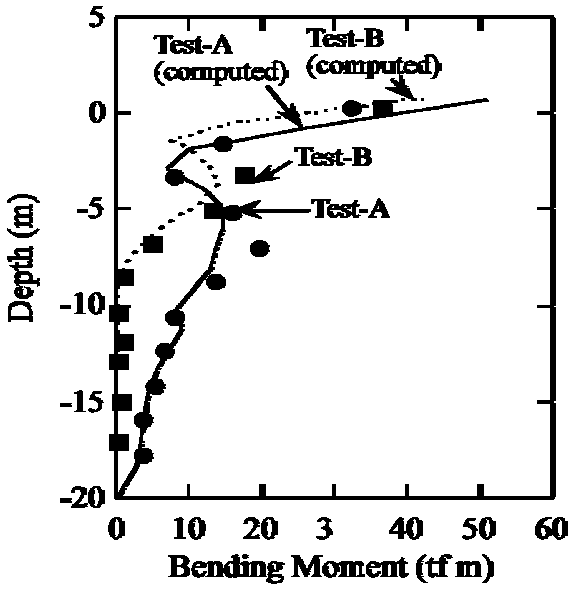

Figure 8: Comparisons of the measured and calculated maximum pile bending moments for Test-A and Test-B

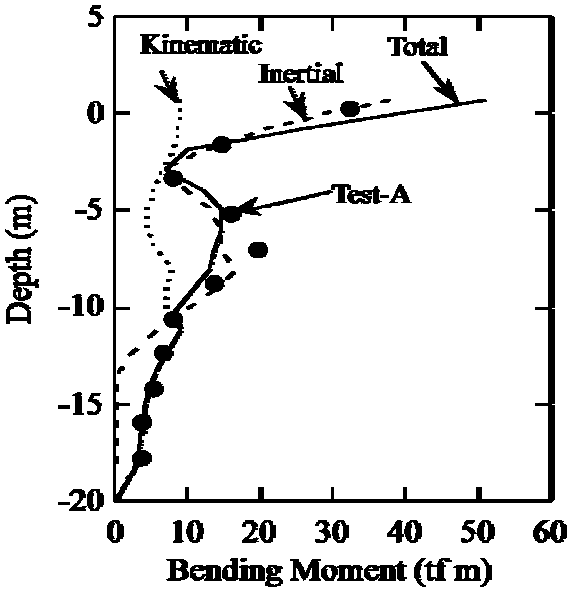

Figure 9: Comparisons of the calculated inertial and kinematic component in maximum pile bending moments for Test-A

be considered to be very weak. Therefore, it is concluded that the pore water pressure was generated almost entirely by earthquake motion. There were minor differences between pore water pressures recorded in the middle of the pile group (P5, P7) and those in the surrounding soil (P4, P6) at each corresponding depth. It seems that the existence of a pile group has little effect on the generation of excess pore water pressure during an earthquake.

Figure 7 compares the time histories of the accelerations, the pile bending moments and the excess pore water pressure ratios for Test-A with the analytical results. The analytical results are in good agreement with test results. The pore water pressure at GL-1.4m (P6) began to increase at around 1.5 seconds and reached 100% liquefaction at around 5 seconds. The pore water pressure at GL-9.0m (P3) also began to increase at around 1.5 seconds, but complete liquefaction did not occur. The acceleration at GL-0.7m in the soil (AH11) was lower in the high frequency component due to the occurrence of liquefaction. Furthermore, from the middle of the wave, a pulse wave occurred due to the cyclic mobility of the soil. The response acceleration of the structure (AH13) contained few high frequency components, and large responses occurred from 2 to 5 and 11 to 12 seconds. The pile bending moment at GL+0.8m(SG11) resembled the acceleration response of the structure in terms of wave shape and became large in the same periods. The pile bending moment at GL-14.8m (SG5), however, contained relatively high frequency components and was rather similar to the input acceleration (AH2). It can be considered that the pile bending moment in the deeper regions of the soil was largely influenced by the response of the soil deposits. Cyclic mobility had little influence on the response of structure and the pile bending moment. The analyses predict well the test results, including the variation with time of acceleration, excess pore water pressure and the pile bending moments at various depths.

2.4 Pile bending moment

The distributions of the maximum pile bending moments were studied to investigate the effect of the inertial force and displacement of the soil deposits on pile bending moments. The moment induced by the inertial force, hereafter called 'inertial component', and the moment caused by the soil displacement, hereafter called 'kinematic component', were calculated independently. The kinematic components were evaluated by the same analytical procedure using a pile foundation model with a massless structure. The inertial components were obtained by subtracting the kinematic components from the total bending moments in the time domain. It is necessary to bear in mind that this procedure is not rigorous as the soil was not in a linear elastic condition during Test-A.

Figure 8 compares the differences between the shaking table test in Test-A and the lateral loading test in Test-B. Figure 9 shows the inertial and kinematic components of the bending moment separated from the total bending moment for Test-A. These figures compare the test results with the analytical results.

In Test-B, the maximum bending moments became large at the pile head and at around GL-4m, which is consistent with the distribution of a fixed head pile under lateral loading at the pile head. In Test-A, the moments

were large from the pile tip to the pile head. They became particularly large at the pile head and at around GL-6m. As shown in Figure 9, the inertial component extended from the pile head to GL-13m. The kinematic component extended from the pile tip to the pile head. As shown in Figure 7, the maximum pile bending moments occurred during the generation of excess pore water pressure. It is confirmed that the inertial component extended deeper than in Test-B, and the kinematic component occurred due to the increase in soil displacement by the decrease of soil rigidity in liquefied soil.

3. PERFORMANCE EVALUATION OF PILE FOUNDATION

Earthquake response analyses of a structure supported on a pile group were conducted to study the method of evaluating pile foundation performance. Pile bending moments are calculated considering pile group effects and the contribution of axial-force fluctuation in the piles. Pile foundation performance is discussed on the basis of pile curvature(ϕ) and pile foundation deformation (Δu), as shown in Figure 10.

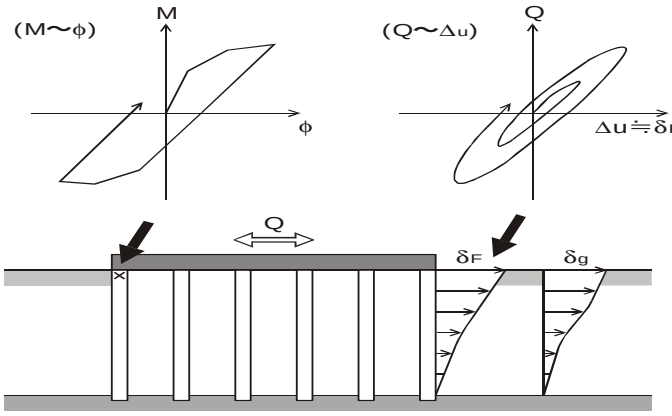

Figure 10: M – ϕ relation of pile and Q – Δu relation of pile foundation

3.1 Superstructure-pile foundation model

The numerical model of the soil-pile foundation-superstructure system used in this study is shown in Figure 11. The piles are modeled as multiple sticks with lumped masses and beam elements. The bending stiffness of the piles is analyzed taking into account the nonlinear relationship between bending moment and curvature dependent on axial force [8]. In this study, interaction soil springs $[K_{pp}]$ are employed to take into account complete pile-soil-pile interactions, as described in 2.2 above. The superstructure is modeled as one stick with lumped masses and beam elements with nonlinear characteristics. The axial force in pile distributes the

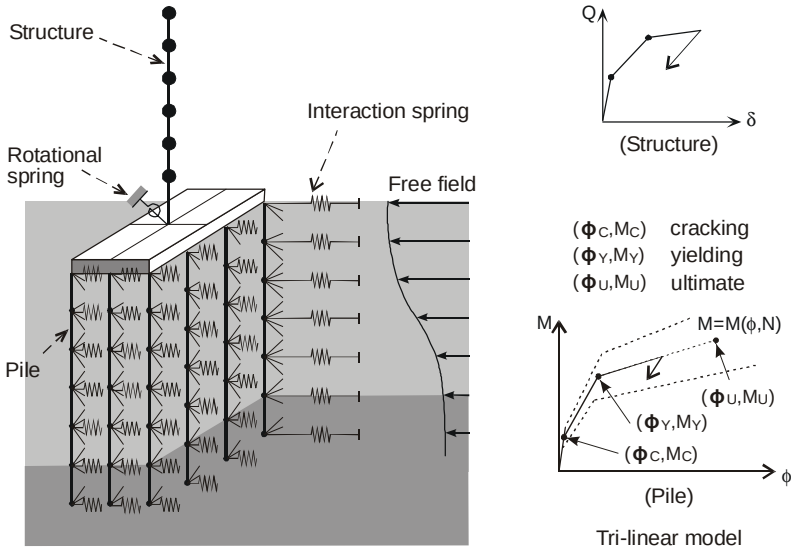

Figure 11: Numerical model of soil-pile foundation-superstructure system

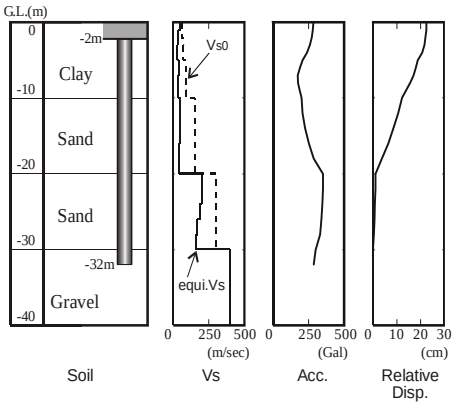

Figure 12: Soil profile and response results

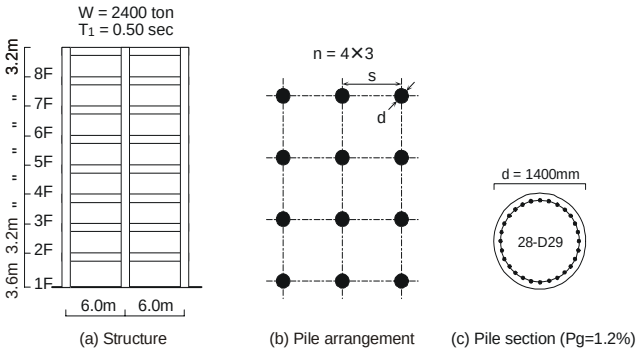

Figure 13: Superstructure and pile model

overturning moment of superstructure as a triangular distribution at each pile position. Figure 12 shows the soil profile in this study and the response results of soil obtained by an equivalent linear analysis. An artificial earthquake (BCJ-L2) is adopted as an input ground motion at GL-30m, which corresponds to a pile-supported layer. The maximum acceleration of the input ground motion is 355.7 Gal. Figure 13 shows the superstructure model and pile arrangement. The superstructure comprises an eight-storied RC building supported by a total of 12 cast-in-place concrete piles. The RC pile is 1.4m in diameter with a steel ratio of 1.2%. The pile heads are rigidly connected to the foundation slab at GL-2.0m.

3.2 Bending moment of pile group

Figure 14 shows the distributions of maximum bending moment and ductility factor of Pile-1, Pile-2, Pile-3 and Pile-5. The ductility factor μ ($= \mu_{max} / \mu_y$) of a pile is defined as the ratio of maximum curvature to that for yield moment of a steel bar. These results indicate that pile responses vary for different locations. Pile-1 and Pile-3, at the corner of the foundation, show larger responses than the internal piles. The

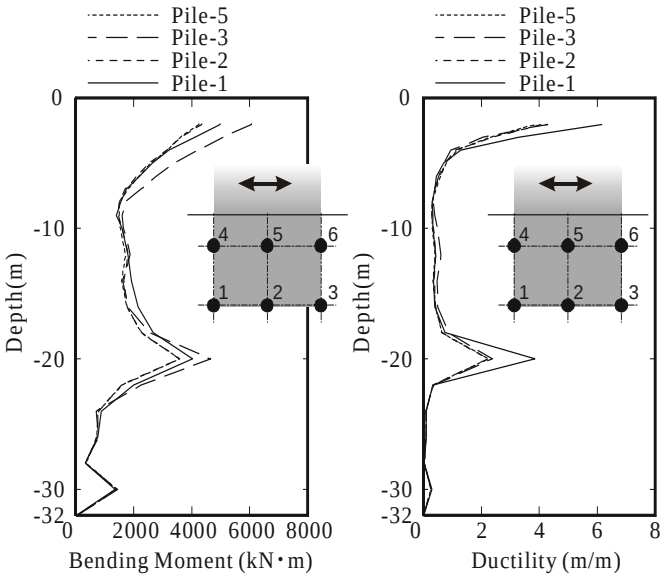

Figure 14: Distributions of maximum bending moment and ductility factor of Pile-1, Pile-2, Pile-3 and Pile-5

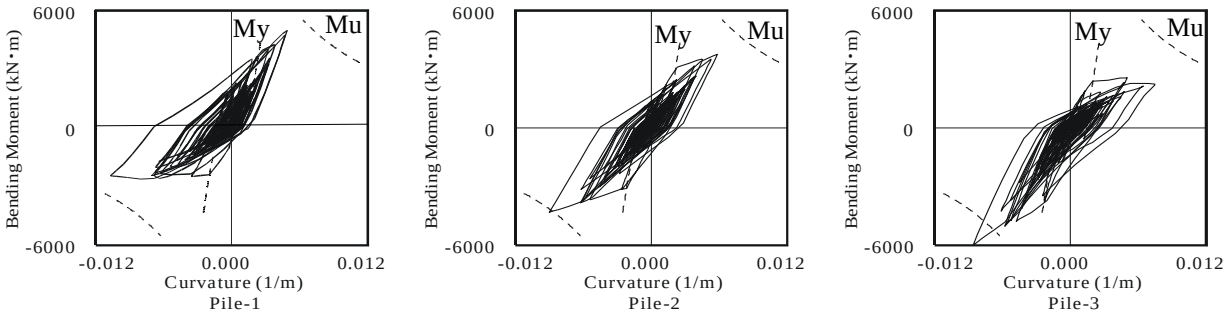

Figure 15: Relationship between bending moment and curvature of Pile-1, Pile-2 and Pile-3

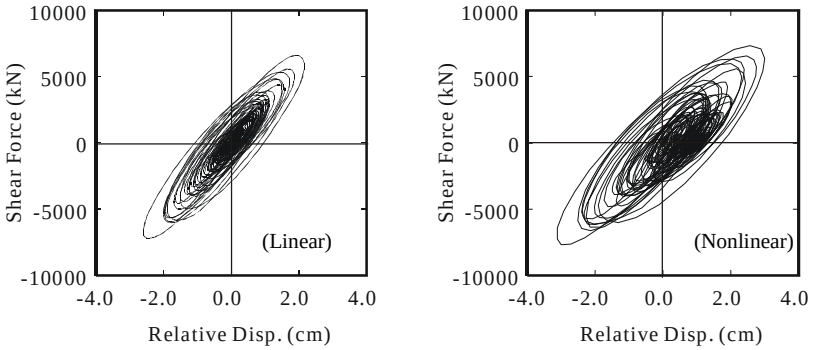

Figure 16： Relationship between shear force at pile head and relative displacement of pile foundation

differences of pile responses occur not only at the pile head but also at the boundary of the soil layer (GL-20m). As described before, the pile bending moment near the pile head is induced by the inertial force of the superstructure, and that at the soil boundary is induced by soil displacement.

Figure 15 shows the hysteretic loops of the relationship between bending moment (M) and curvature(ϕ) of Pile-1, Pile-2 and Pile-3. The pile response in compression increases in strength but decreases in deformation capacity. Then Pile-3, at the corner, reaches the ultimate moment (Mu) during compressive loading. However, the pile response in tension increases in deformation capacity. Then the ductility factor of Pile-1 becomes larger than those of other piles during tensile loading. Each pile response in pile group differs by reason of both pile group effect due to pile-soil-pile interaction and the difference of nonlinear characteristics that depend on the axial force. Pile-soil-pile interaction becomes smaller because of nonlinearity of the surrounding soil. Therefore, in performance evaluation of pile group, it is important to take into account the deformation capacity of a pile dependent on the axial force.

Pile foundation deformation is another significant factor in evaluating its performance. Figure 16 shows the relationship between shear force (Q) at pile head and relative displacement (Δu) of the pile foundation. The left side of the figure shows the results where piles are assumed to be linear and the right one shows the results where piles have nonlinear characteristics that depend on the axial force. Horizontal relative displacement (Δu) almost corresponds to the difference between pile foundation and free ground. It is confirmed that pile foundation displacement varies with the degree of pile nonlinearity. It is necessary to rationally evaluate the relation between pile foundation performance level and displacement depended on pile nonlinearity.

4. CONCLUSIONS

The concluding remarks of these centrifuge tests and analytical studies are as follows:

1. Pile bending moments near the pile head are greatly affected by the inertial force of the structure, and the inertial component reaches deeper in the pile under soil nonlinearity. The kinematic component occurs due to the increase in soil displacement induced by liquefaction, and extends from the pile tip to the pile head.

2. The proposed numerical model of the soil-pile group foundation system, which consists of beam elements and nonlinear interaction springs, is verified by simulation analyses of the centrifuge tests. It is confirmed that this proposed model well represents pile foundation response in liquefied soil.

3. To evaluate pile foundation performance it is important to precisely predict pile curvature and pile foundation deformation using a complete soil-pile foundation-superstructure system. Bending moment and curvature of piles are greatly influenced by nonlinear characteristics that depend on the axial force. Pile foundation displacement also depends on pile nonlinearity. It is necessary to rationally evaluate the relation between performance and pile foundation displacement.

5. ACKNOWLEDGEMENTS

The author wishes to express his appreciation to Dr. Sako and Dr. Adachi of Kajima Corporation for their fruitful discussions and cooperation.

6. REFERENCES

1) Miyamoto Y., Sako Y., Miura K., Scott R. F. and Hushmand B., (1992): Dynamic behavior of pile group in liquefied sand deposits, Proc. of 10WCEE, 3, pp.1749-1754
2) Miyamoto Y., Sako Y., Kitamura E. and Miura K., (1995): Earthquake response of pile foundation in nonlinear liquefiable soil deposit, J. Struct. Constr. Eng., AIJ, No.471, pp.41-50
3) Miyamoto Y., Fukuoka A., Adachi N. and Koyamada K., (1997): Pile response induced by internal and kinematic interaction in liquefied soil deposit (Centrifuge model test for pile foundation in saturated sand layers and its analytical study, J. Struct. Constr. Eng., AIJ, No.494, pp.51-58
4) Adachi N., Miyamoto Y. and Koyamada K., (1998): Shaking table test and lateral loading test for pile foundation in saturated sand, Is-Tokyo Centrifuge '98, pp.289-294
5) Ishihara K. and Towhata I., (1980): One-Dimensional Soil Response Analysis during Earthquakes Based on Effective Stress Method, Jour. of Faculty of Eng., Univ. of Tokyo, Vol.135, No.4
6) Kausel E. and Peek R., (1982): Dynamic loads in the interior of a layered stratum -An explicit solution, Bulletin of the Seismological Society of America, 72, pp.1459-1481
7) Broms B. B., (1965): Design of laterally loaded piles, Journal of the Soil Mechanics and Foundation Division, ASCE, 91, pp.79-99
8) Sako Y. and Miyamoto Y., (1999): Earthquake response of pile foundation considering contribution of axial-force fluctuation in piles, J. Struct. Constr. Eng., AIJ, No. 523, pp.79-86